Ion Implantation into Race Surfaces of Aerospace Ball Bearings in a Plasma Immersion Configuration

Zhaoming Zeng, Paul K. Chu, *Senior Member, IEEE*, Xiubo Tian, Baoyin Tang, and Dixon Tat-Kun Kwok, *Member, IEEE*

***Abstract*—Plasma immersion ion implantation (PIII) is an effective technique to improve the surface properties of industrial components possessing an irregular shape, such as ball bearings used in the aerospace industry. The implant uniformity and efficiency along both the inner and outer races of a ball bearing assembly is investigated experimentally and theoretically. We study the sample placement as well as different PIII processing conditions. The use of a three-dimensional (3-D) model to investigate the influence of the sample stage on the implantation efficiency and dose uniformity is described. Based on the experimental results, under typical PIII conditions, the dose variation along the outward-facing groove of the inner ring of the ball bearing assembly is 60%, whereas that along the inward-facing groove of the outer ring is 51%. By using a shorter pulsewidth and higher plasma density, the nonuniformity is improved to about 35%, which is acceptable to the aerospace industry. The experimental observations are in agreement with simulation results, and the improvement can be attributed to the better conformability of the plasma sheath to the race surface. Our results demonstrate the viability of PIII to enhance the surface properties of both the inner and outer rings of industrial ball bearings.**

***Index Terms*—Bearings, implantation uniformity, plasma immersion ion implantation, sheath simulation.**

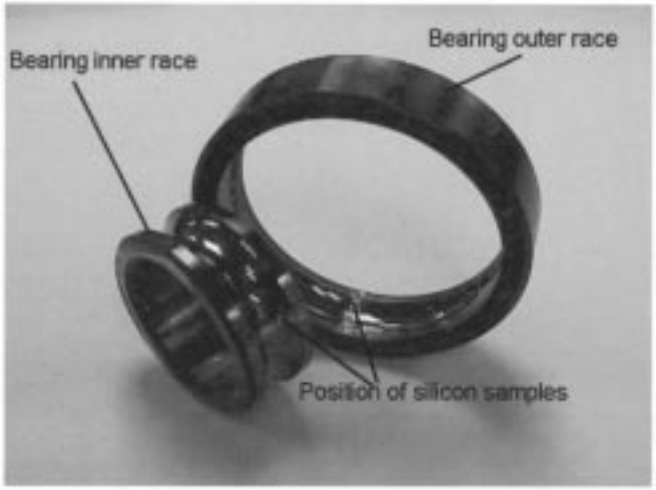

Fig. 1. Photograph of the inner and outer rings of the ball bearing assembly. The "white" square spots shows the locations where the silicon samples were originally affixed. The silicon samples were subsequently measured by Auger electron spectroscopy to disclose the implant in-depth distributions and retained doses.

I. Introduction

PLASMA immersion ion implantation (PIII) is a nonline-of-sight technique for the surface modification of industrial components [1]–[4]. One of its advantages over conventional ion beam implantation is the capability to efficiently treat irregular-shaped samples without complex sample or ion beam manipulation. Moreover, as almost no dimensional changes exist after PIII treatment, the technique excels in the enhancement of the surface properties of mechanical parts having strict dimensional tolerances. It is also an effective alternative technique to improve the performance of components used in space when conventional coatings and surface treatment technology may encounter difficulties in the vacuum environment. Consequently, it is an excellent treatment process for precision bearings used in satellites.

Implant uniformity is an important factor not only affecting the efficacy of the treatment process, but also the acceptance of PIII by the industry. As a result, theoretical and experimental studies have been performed on specimens of various shapes [5]–[12]. Malik *et al.* [9] determined the implanted nitrogen concentration into a wedge-shaped target to study the influence of the target edges on the energy and spatial distribution of the implanted ions. Hartmann *et al.* [10], [11] investigated the PIII homogeneity of wedge-specimens (V- and D-shaped) with different angles, and Mandl *et al.* [12] measured and calculated the PIII dose distribution on cylindrical samples, such as drill bits possessing different diameters. The results of these studies reveal that the PIII dose varies substantially with different target shapes. Hence, an independent investigation must be conducted for each kind of samples. For ball bearings used in aerospace applications, the working surfaces are the races on which the balls roll. The arc surfaces are difficult to treat because of the nonplanar geometry, especially the inward-facing race on the outer ring. In addition, the use of conventional lubricants and coatings may not be compatible with the vacuum and high UV environment in space. In this respect, surface modification by means of ion implantation employing a plasma immersion mode possesses some distinct advantages. In this work, we conduct a comprehensive study on the implantation process into the arc surfaces of both the inner and outer pieces of such a ball bearing assembly. The effects of instrumental parameters, such as the pulsewidth and plasma density on the implantation process, are also investigated. To understand the experimental results, simulation is conducted using two- and three-dimensional (2-D and

Manuscript received August 10, 1999; revised October 26, 1999. This work was supported by the Hong Kong Research Grants Council, under earmarked grants 9040332, 9040344, and 9040412, and the City University of Hong Kong, under Strategic Grant 7000964.

The authors are with the Department of Physics and Material Science, City University of Hong Kong, Kowloon, Hong Kong (e-mail: paul.chu@cityu.edu.hk).

Publisher Item Identifier S 0093-3813(00)03664-X.

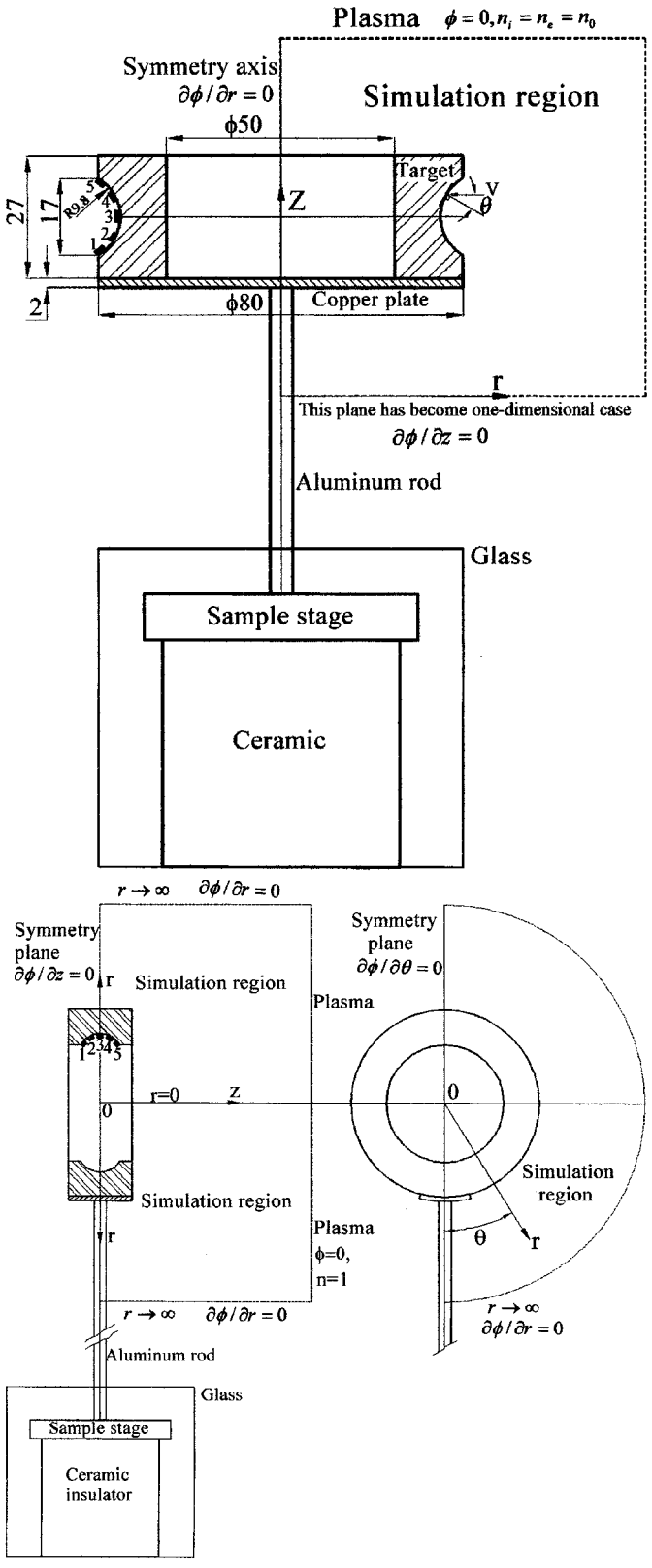

Fig. 2. Schematic of PIII experimental setup, simulation region, and sample placement (dimensions in millimeters) for the (a) inner ring with the outward-facing race and (b) outer ring with the inward-facing race.

3-D) fluid models to study the relationship between the plasma sheath evolution and implant dose uniformity.

TABLE I
EXPERIMENTAL PARAMETERS OF THE THREE PIII TREATMENT PROCESSES

PIII Parameters	Case 1	Case 2	Case 3
Implantation voltage	-20 kV	-20 kV	-20 kV
Pulse width	10 μs	10 μs	5 μs
Pulse repetition rate	200 Hz	200 Hz	300 Hz
Gas Pressure	2.2×10^{-2} Pa	2.2×10^{-2} Pa	2.2×10^{-2} Pa
Filament discharge current	1 A	0.5 A	1 A
Filament discharge voltage	90V	90V	90V
Measured plasma density	3.5×10^{9} cm^{-3}	2.2×10^{9} cm^{-3}	3.5×10^{9} cm^{-3}
Implantation time	2 hours	2 hours	2 hours

II. EXPERIMENTAL

A 9Cr18 stainless steel (AISI440) ball bearing (model 310) with an interior diameter of 50 mm was processed in a a multipurpose plasma immersion ion implanter [13]. As shown in Fig. 1, the ball bearing assembly comprises two rings. The smaller ring with the race facing outward is the inner piece, whereas the bigger ring with the race surface facing inward constitutes the outer piece. During normal operation, rotating actions are sustained by metal balls rolling between the two grooves. Hence, the surface properties of the race surfaces, such as hardness and lubricity, are thus critical to the performance of the ball bearing. To study the implant dose variation along the two race surfaces, pieces of silicon (2 mm $\times$ 3 mm) were affixed using conductive silver paint onto the arc surfaces, as exhibited in Fig. 2(a) and (b). For best results, we placed the two rings in the vacuum chamber in different orientations. As shown in Fig. 2(a), the inner ring of the assembly with the race facing outward was placed horizontally on a copper plate 2 mm thick having the same diameter as the ring. The plate was erected from the sample stage by a 6-mm diameter, 500-mm long aluminum rod. This configuration has been shown to yield the best implant uniformity while not draining excessive current from the power modulator [14]. The outer ring of the bearing with the race facing inward was placed vertically on a metal support with an arc trench erected from the sample stage, as shown in Fig. 2(b). To minimize the influence of the sample stage and decrease the total implantation current, a glass shroud was used to cover the stage. Before the experiments, the vacuum chamber was pumped down to a base pressure of 8×10^{-4} Pa. A nitrogen plasma was ignited using a glow discharge filament source. Experiments were conducted under three different conditions to investigate the influence of the pulsewidth and plasma density on the implant uniformity. The experimental conditions are summarized in Table I. The plasma density was experimentally measured by a Langmuir probe before each PIII experiment. After PIII, the silicon samples were analyzed using Auger electron spectroscopy (AES) to acquire the nitrogen depth profiles as well as to calculate the implantation doses at various locations along the two groove surfaces. The Auger analysis was performed using a Physical

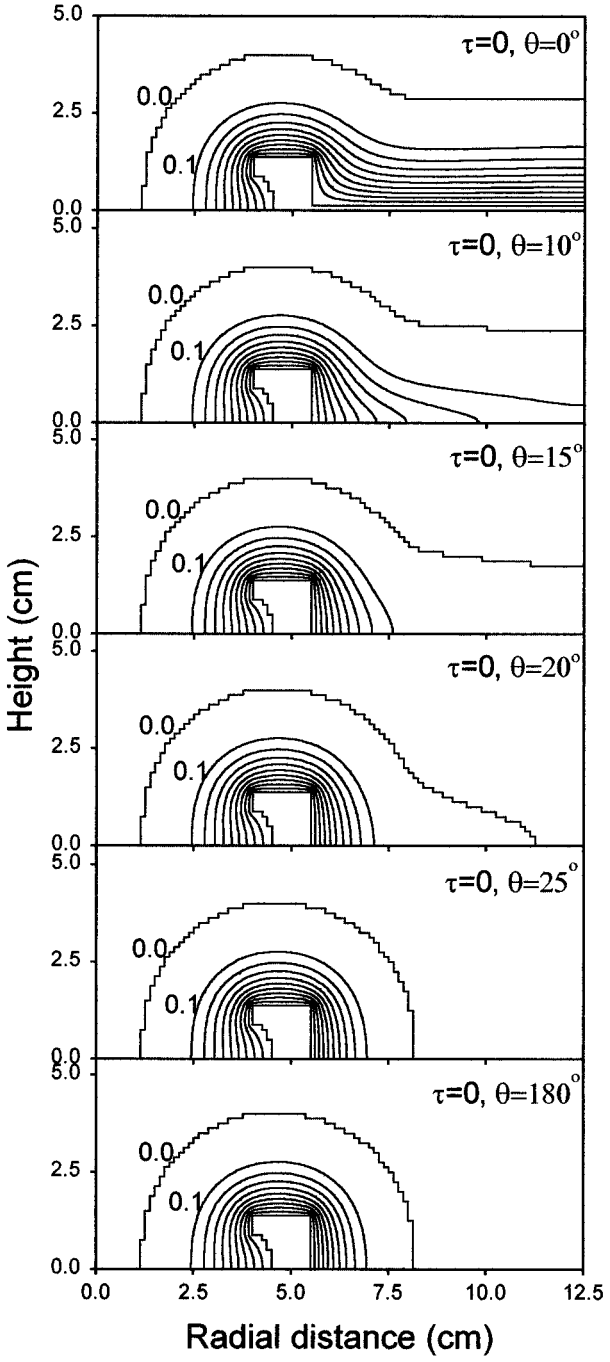

Fig. 3. Equipotential contours of the ion-matrix sheath formed at $t = 0$ around the bearing outer ring at different angles, θ [Fig. 2(a)].

Electronics PHI-610 instrument. The primary electron energy was 3 keV, and the impact angle was 30°. Sputtering was achieved using an argon ion beam. The sputtering rate of 30 nm/s was estimated based on analysis of previous samples, but because the sputtering rate is not expected to be uniform throughout the profile, the Auger depth scales are not accurate, but sample-to-sample comparison is more valid. The retained doses are calculated by integrating the area under the quantified profiles (by archival relative sensitivity factors), and they are approximate as well.

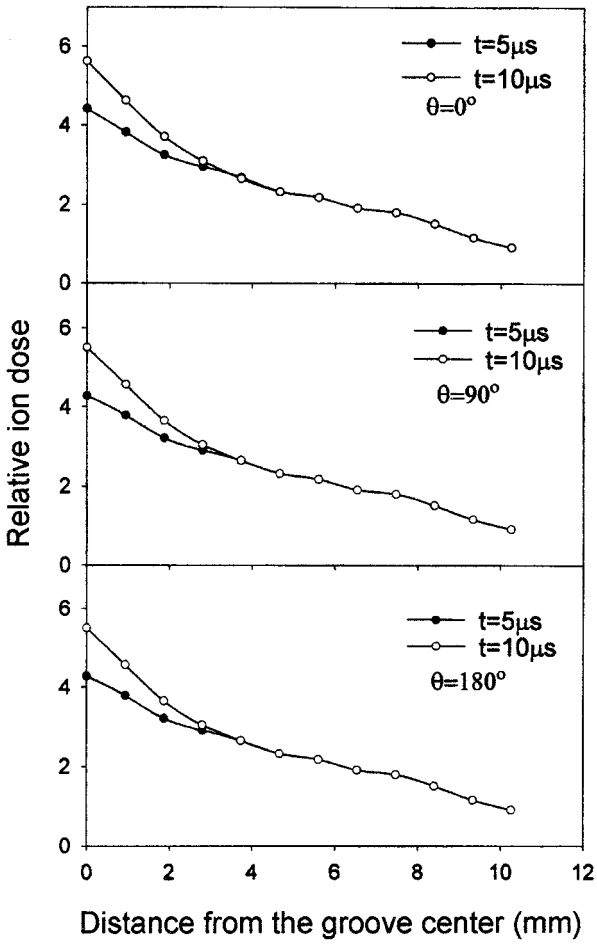

Fig. 4. Simulated incident ion doses along the groove surface of the bearing outer ring for different angle and pulsewidths.

III. Theoretical Simulation

PIII into the two bearing rings is investigated by modeling the temporal sheath expansion using a fluid model. To better reflect the real situation, the supporting rod is included in the simulation model. For the bearing inner ring shown in Fig. 2(a), a 2-D model is adequate to simulate the PIII sheath properties on account of its axial symmetry. However, for the bearing outer ring illustrated in Fig. 2(b), no apparent symmetry exists, and so a 3-D model in cylindrical coordinates is adopted. It should be noted that the computational power and capacity required by 3-D simulation are large, and very few 3-D simulation results have hitherto been reported. However, in reality, most real samples and sample stage are 3-D and we have adopted a 3-D approach in this work. In the typical sub-mTorr pressure range used in PIII, the average mean free path is much larger than the sheath thickness, and so the PIII process can be described by a collisionless, cold plasma fluid model. The evolution of the ion densities n_i, ion velocity v_i, and electric potential ϕ can be modeled using cold, collisionless fluid ions, Boltzmann electrons, and Poisson's equation [8], [15]–[19]. In cylindrical coordinates, the 3-D equations of ion continuity and motion, Poisson's equation, and Boltzmann relationship are

$$\frac{\partial n}{\partial \tau} + \frac{1}{R}\frac{\partial}{\partial R}(Rnu_R) + \frac{1}{R}\frac{\partial}{\partial \theta}(nu_\theta) + \frac{\partial}{\partial Z}(nu_Z) = 0 \qquad (1)$$

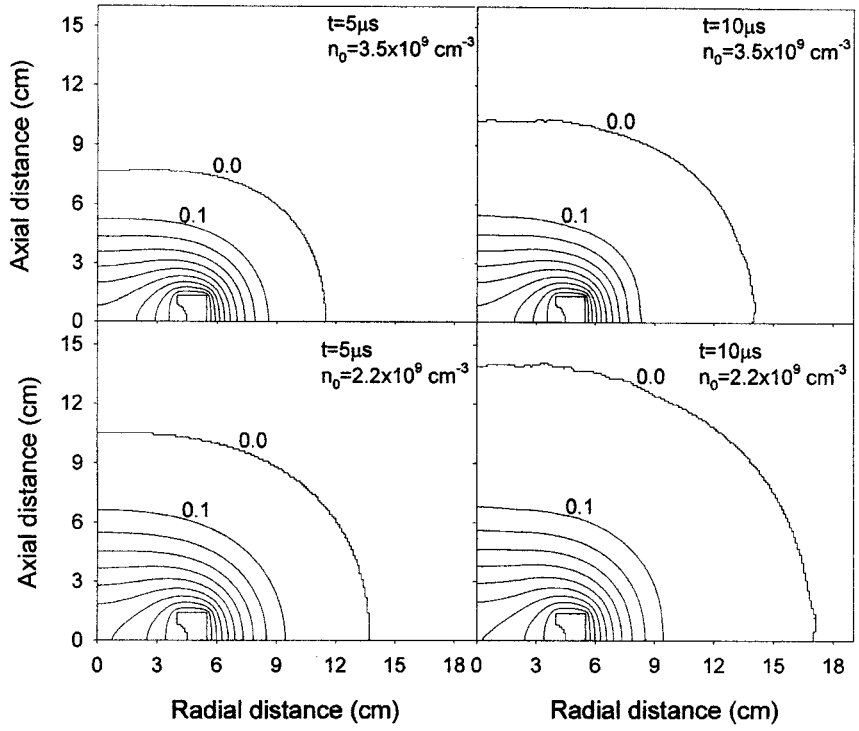

Fig. 5. Normalized potential distribution around the bearing outer ring for different implantation pulsewidths and plasma densities.

$$\frac{\partial u_R}{\partial \tau}+u_R\frac{\partial u_R}{\partial R}+\frac{u_\theta}{R}\frac{\partial u_R}{\partial \theta}+u_Z\frac{\partial u_R}{\partial Z}=\frac{1}{2}\frac{\partial \psi}{\partial R} \tag{2a}$$

$$\frac{\partial u_\theta}{\partial \tau}+u_R\frac{\partial u_\theta}{\partial R}+\frac{u_\theta}{R}\frac{\partial u_\theta}{\partial \theta}+u_Z\frac{\partial u_\theta}{\partial Z}=\frac{1}{2r}\frac{\partial \psi}{\partial \theta} \tag{2b}$$

$$\frac{\partial u_Z}{\partial \tau}+u_R\frac{\partial u_Z}{\partial R}+\frac{u_\theta}{R}\frac{\partial u_Z}{\partial \theta}+u_Z\frac{\partial u_Z}{\partial Z}=\frac{1}{2}\frac{\partial \psi}{\partial Z} \tag{2c}$$

$$\frac{1}{R}\frac{\partial}{\partial R}\left(R\frac{\partial \psi}{\partial R}\right)+\frac{1}{R^2}\frac{\partial^2 \psi}{\partial \theta^2}+\frac{\partial^2 \psi}{\partial Z^2} =2\left[n-\exp\left(\frac{e\phi_t}{KT_e}\cdot\psi\right)\right]. \tag{3}$$

The normalized dimensionless variables are

$$\begin{aligned} R&=x/s_0,\ \ Z=z/s_0,\ \ \psi=\phi/\phi_t,\ \ n=n_i/n_o\\ u_R&=v_{ir}/v_{\max},\ \ u_\theta=v_{i\theta}/v_{\max},\ \ u_Z=v_{iz}/v_{\max}\\ \tau&=t\omega_{pi} \end{aligned} \tag{4}$$

where

$s_0 = \sqrt{-2\varepsilon_0\phi_t/en_0}$ is the planar ion-matrix sheath width;

$v_{\max} = \sqrt{-2e\phi_t/m}$ is the velocity that an ion would gain if it fell through a potential drop ϕ_t;

$w_{pi} = \sqrt{n_0e^2/\varepsilon_0 m}$ is the ion plasma frequency.

For the 2-D model in cylindrical coordinates [14], [21], we let $u_\theta = 0$, and $\partial/\partial\theta = 0$ in (1)–(3). The simulation regions for the inner and outer rings are depicted in Fig. 2. The initial conditions are $n = 1$ and $u_R = u_z = 0$ everywhere. The boundary conditions are $\psi = 1$ on the target and $\psi = 0$ in the plasma. In Fig. 2(a), at the central symmetry axis of the ring, $\partial\psi/\partial r = 0$ and $\partial\psi/\partial z = 0$ at the lower boundary of the simulation region because it is far from the ring and can be treated as a 1-D case. In Fig. 2(b), $\partial\psi/\partial z = 0$ at the r-z symmetry plane of the ring. On the r-θ plane, the left boundary is the symmetry plane of the ring, and so $\partial\psi/\partial\theta = 0$. The arc boundary is $r \to \infty$ and $\partial\psi/\partial r = 0$ at this boundary. For the 2-D model, the potential along the $r = 0$ axis can be calculated using Hospital's rule [20]. However, for the 3-D model, the calculation of the potential along the $r = 0$ axis is much more complicated. In the work, the potential along this axis is determined using a finite difference method in rectangular coordinates and deriving the average values along the plane at different angles. To verify the validity of our 3-D model, the PIII process of a symmetrical 3-D target (that is, a 2-D one in reality) is simulated and compared with the results obtained by a 2-D model using Hospital's rule [20]. The two sets of results are consistent. The simulation parameters are the same as the actual experimental parameters described in Table I. The simulation is conducted to a final time of $t = 10$ μs.

IV. Results and Discussion

A. Simulation Results

Fig. 3 shows the potential distribution of the ion-matrix sheath formed at $t = 0$ around the bearing outer ring at different angles (θ) using the PIII experimental parameters described in case 1 of Table I. It is found that when the angle is more than 25°, the potential distribution is hardly influenced by the supporting rod. Hence, the region influenced by the supporting rod is only within $\pm 25°$. Moreover, the supporting rod only affects the sheath distribution around the exterior wall of bearing ring. Our results show that no influence on the sheath distribution exists around the groove of the outer ring.

Fig. 4 displays the simulated ion dose distribution along the groove of the outer ring at different angles and pulsewidths. The

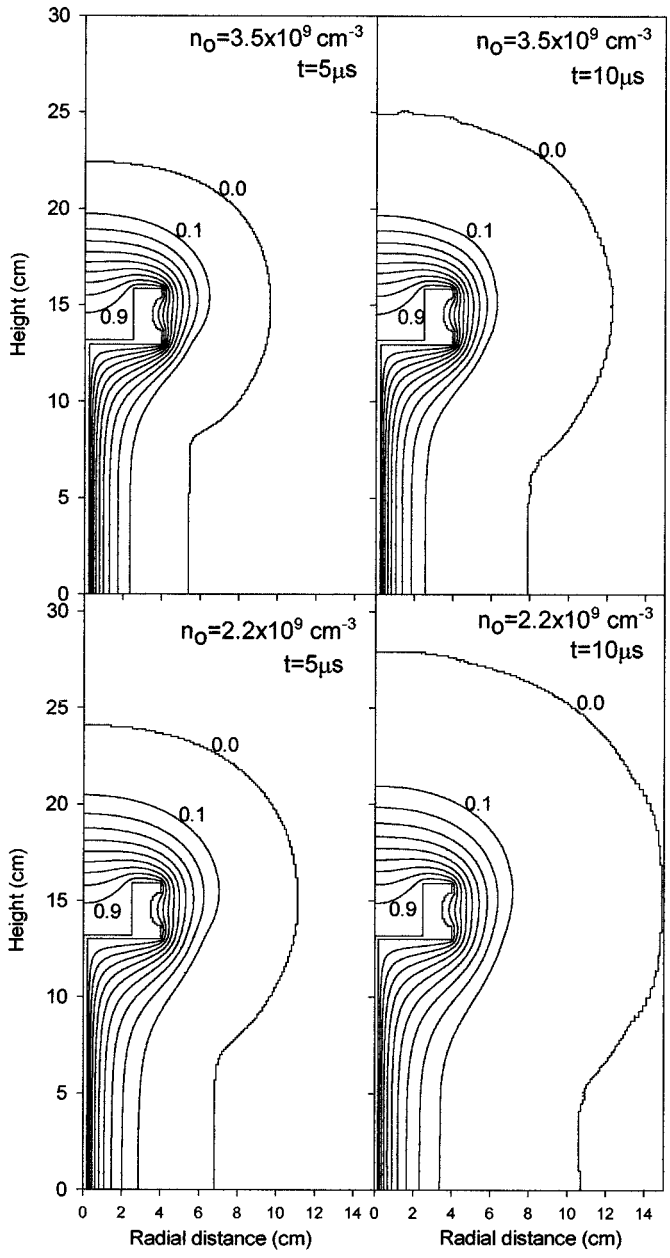

Fig. 6. Normalized potential distribution around the bearing inner ring for different implantation pulsewidths and plasma densities.

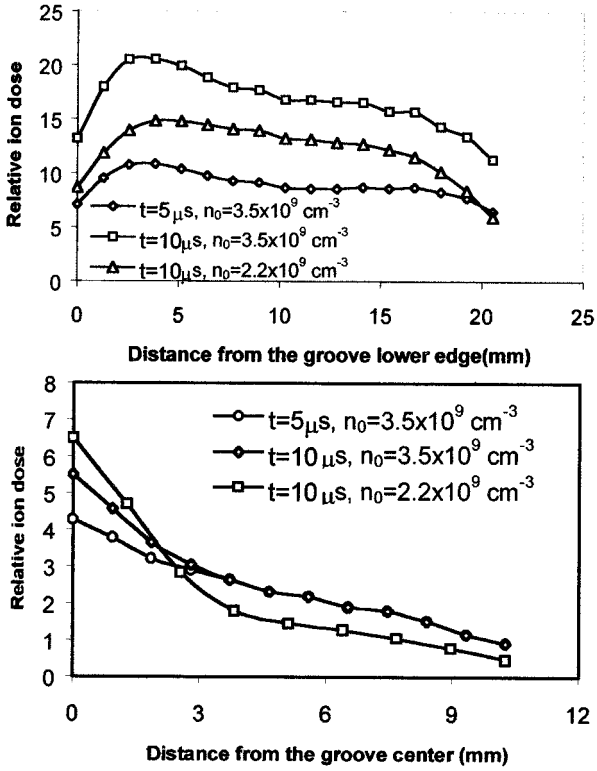

Fig. 7. Simulated incident ion doses along the groove surface of bearing inner and outer rings for different implantation pulsewidths and plasma densities: (a) inner ring with the outward-facing race and (b) outer ring with the inward-facing race.

ion dose is almost the same at different angles. Therefore, the supporting rod has almost no adverse affects and is in fact beneficial to the PIII treatment of the groove surface of the outer ring as it eliminates sample stage effects. Fig. 4 also shows that when the pulsewidth is increased, the lateral ion dose uniformity along the groove surface becomes worse.

Fig. 5 exhibits the potential distribution around the bearing outer ring at $\theta = 90°$ at different pulsewidths and ion densities. When $t = 10$ μs and $n_o = 2.2 \times 10^9$ cm^{-3}, the sheath expansion is the largest and the sheath is the thickest. When $t = 5$ μs and $n_o = 3.5 \times 10^9$ cm^{-3}, the sheath thickness is the smallest. Thus, it can be observed that the conformality of the sheath to the target surface is better when using a shorter pulsewidth and higher plasma density. Better conformality leads to more uniform ion implantation into the groove surface of the bearing.

Fig. 6 depicts the potential distribution around the bearing inner ring at different pulsewidths and plasma densities. Results similar to those obtained on the outer ring are obtained. That is, a longer pulsewidth and lower plasma density result in larger sheath expansion and worse conformality to the target surface.

The simulated ion dose distribution along the groove surface of the inner and outer rings under different PIII conditions are plotted in Fig. 7(a) and (b), respectively. It can be readily observed that the uniformity along the inner and outer race is worst when $t = 10$ μs and $n_o = 2.2 \times 10^9$ cm^{-3} when the sheath expansion is largest.

B. Experimental Results

Fig. 8 displays the Auger nitrogen depth profiles of the five silicon samples affixed to the race of the inner ring [Fig. 2(a)] implanted under the three conditions shown in Table I. In all three cases, the samples near the lips (samples #1 and #5) have smaller projected ranges. Moreover, the variation of the projected ranges is not symmetrical about the center. The samples closer to the supporting copper platen show larger projected ranges. The projected range of sample #4 is smaller than that of sample #2 and the same is true comparing sample #5 with sample #1. The results are in agreement with our previous simulation study [21]. Ions strike the area near the groove edge at large incident angles relative to the normal, resulting in shallower implantation in these locations. Comparing the three processing conditions, although the nitrogen depth profiles are different, the maximum penetration depth does not differ

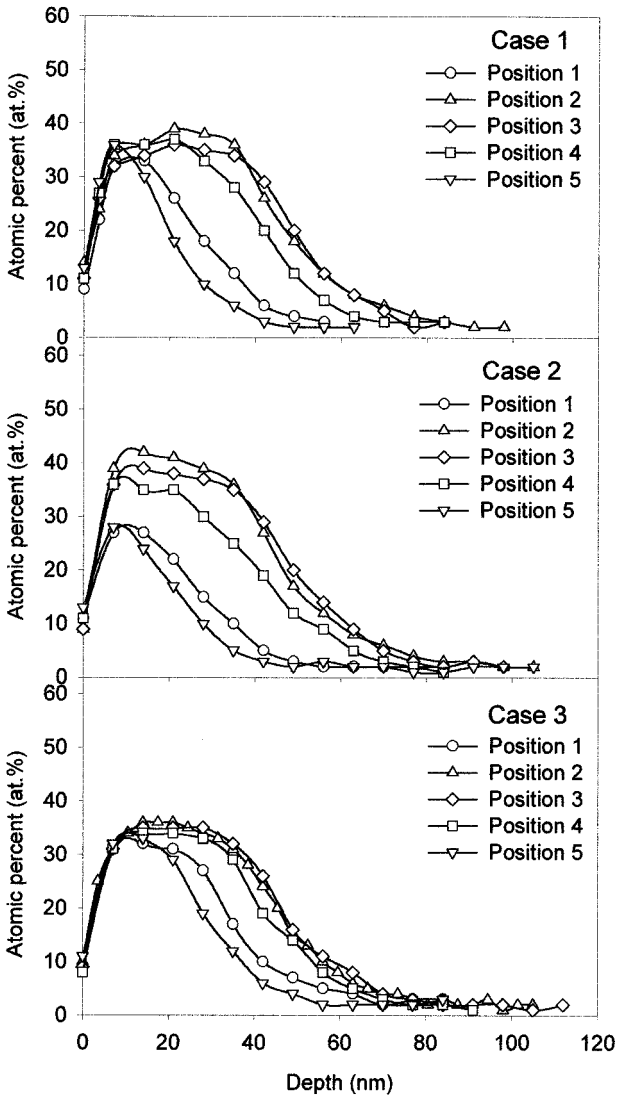

Fig. 8. Nitrogen depth profiles of the five silicon samples affixed on the groove surface of the bearing inner ring shown in Fig. 2(a). The three processing conditions shown in Table I are used: top (Case 1), middle (Case 2), and bottom (Case 3).

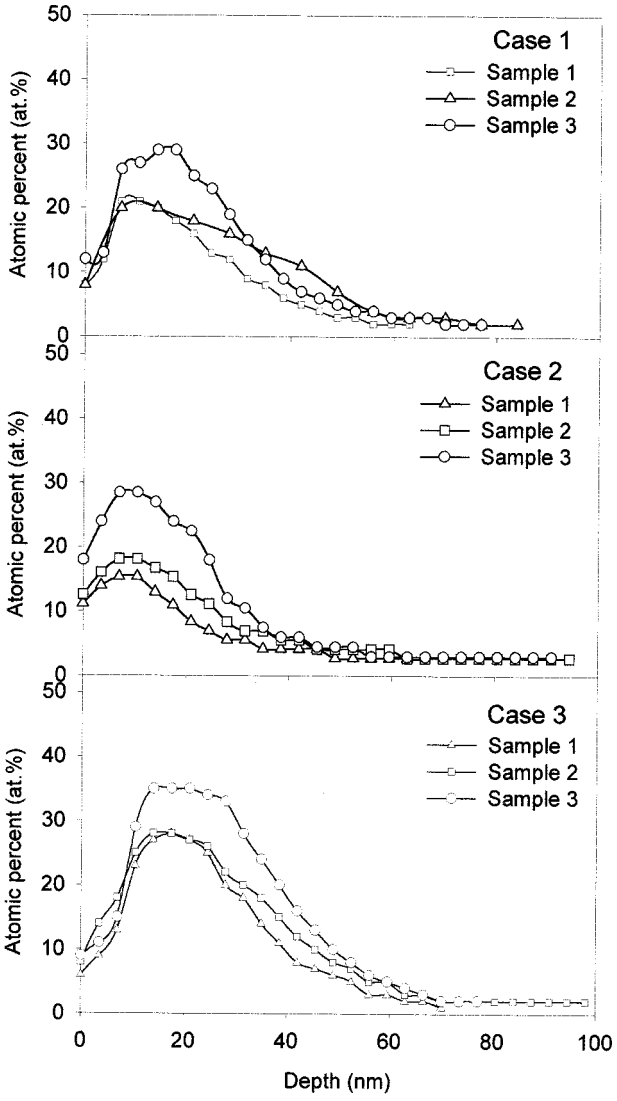

Fig. 9. Nitrogen depth profiles of the three silicon samples affixed on the groove surface of the bearing outer ring shown in Fig. 2(b) (samples #1, #2, and #3). The three processing conditions shown in Table I are used: top (Case 1), middle (Case 2), and bottom (Case 3).

significantly, because of the same implantation voltage used in the three experiments and the low pressure, collisionless conditions.

Fig. 9 shows the nitrogen depth profiles of the silicon samples placed along the race of the outer ring [Fig. 2(b)] for the three processing conditions. As the race surface is sufficiently far away from the supporting Cu plate and the sample holder, minimal variation occurs along the groove surface, for example, between the upper and lower ends. In addition, our sample placement configuration has a vertical symmetry, and we thus only need to measure three samples [samples #1, #2, and #3 shown in Fig. 2(b)] to assess the PIII uniformity along the arc surface. The groove center (sample #3) shows the largest projected range. Comparing the samples implanted using the three conditions, the one treated using a higher plasma density an smaller pulsewidth has the largest projected range. Under the low plasma density and large pulsewidth conditions (case 2), the sheath expands more rapidly, and the ion incident angle is larger, giving rise to shallower implantation and consequently higher sputtering loss or a lower retained dose.

The retained doses measured from the samples placed along the inner ring [Fig. 2(a)] and implanted using the three conditions are shown in Fig. 10. In all three cases, the retained dose is higher near the groove center. The variation of the retained dose is not symmetrical about the groove center. The upper side (samples #4 and #5) shows higher retained dose values. The observation is in agreement with the simulation results. The regions close to the lips (samples #1 and #5) implanted using a short pulsewidth and high plasma density (case 3) have high retained doses compared with the other conditions, and the distribution is more uniform along the groove surface. In case 3, the maximum dose variation is 38%, and in cases 1 and 2, the maximum dose deviation is 55% and 60%, respectively. Our results show that PIII using a shorter pulsewidth and high plasma density yields better uniformity. Another interesting observation is that in cases 1 and 2, sample #2 has a slightly larger retained

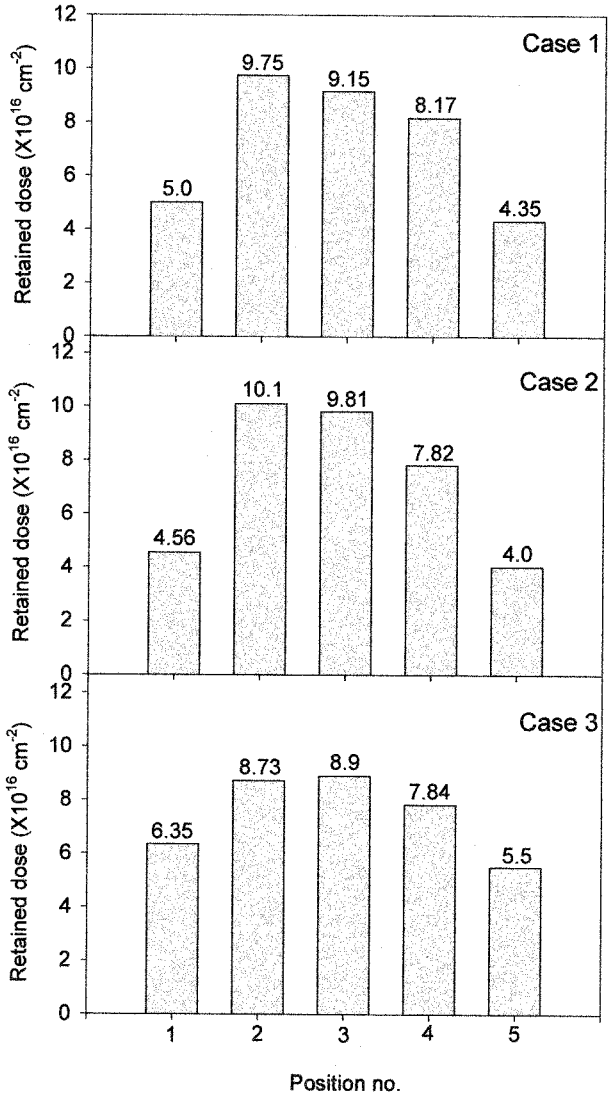

Fig. 10. Experimentally determined retained doses of the five silicon samples affixed on the groove surface of the bearing inner ring shown in Fig. 2(a). The three processing conditions shown in Table I are used: top (Case 1), middle (Case 2), and bottom (Case 3).

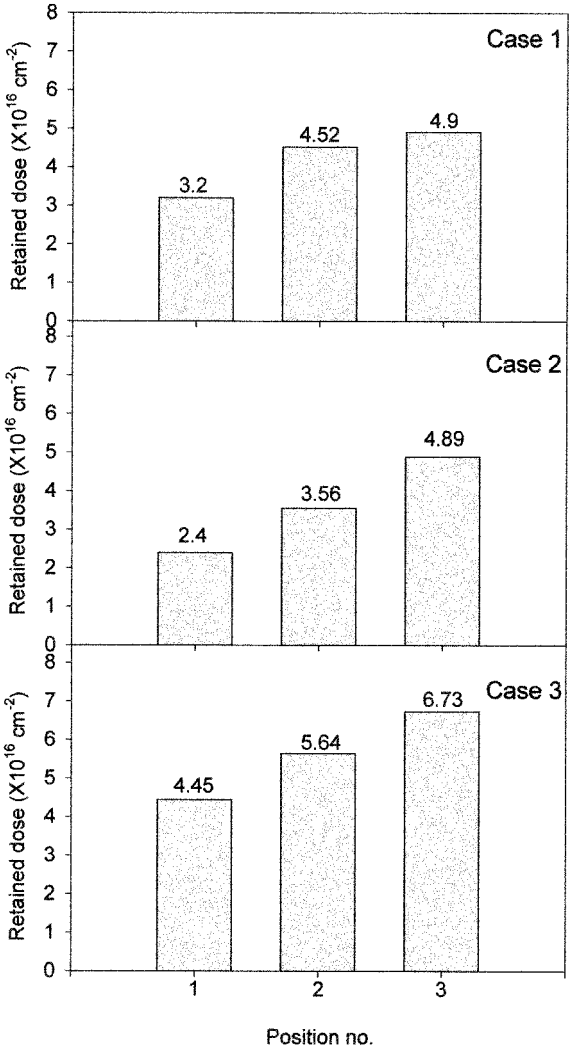

Fig. 11. Experimentally determined retained doses of the three silicon samples affixed on the groove surface of the bearing outer ring shown in Fig. 2(b) (samples #1, #2, and #3). The three processing conditions shown in Table I are used: top (Case 1), middle (Case 2), and bottom (Case 3).

dose than sample #3, but the contrary is true in case 3. Our data show that the larger sheath thickness as a result of the longer pulsewidth leads to a higher number of ions implanted into the lower side of the bearing.

Fig. 11 shows the retained dose distribution along the race of the outer ring [Fig. 2(b)] for the three processing conditions. Not surprisingly, the groove center (sample #3) shows the largest retained dose, and the edge (sample #1) has the smallest retained dose. The samples implanted using a higher plasma density and smaller pulsewidth (case 3) show the largest retained dose values. The maximum variations in the retained doses along the race are 35%, 51%, and 33% for cases 1, 2, and 3, respectively. The high plasma density, small pulsewidth conditions lead to more efficient and uniform implantation. The retained dose values are lowest in case 2, and it is probably because of the larger sheath expansion under the low plasma density, long pulsewidth conditions. In this situation, the ions in the vicinity of the races are depleted quickly because of the low density, and the sheath edge consequently propagates at a high velocity. With a rapidly expanding sheath, ions are drawn in from the outside region and implanted at oblique angles. Hence, even though these ions arrive at the groove surface, many of them are not implanted deep enough and can subsequently be sputtered away.

Comparing the two rings, the retained dose on the inward-facing race surface of the outer ring is lower for the same processing conditions and implantation time. Our results thus show that implantation into the race facing inward is less efficient and more difficult. To achieve the same implant dose, the implantation time must be longer, and a shorter pulse duration and higher plasma density should be used.

The simulation results show that with a longer pulsewidth and lower plasma density, the sheath thickness is larger when the pulse ends. The thicker sheath does not conform to the target shape as well as a thinner one and, in fact, attains a dome shape in the end. The sheath edge, thus, does not reflect the actual shape of the races, and the incident angle becomes more oblique, especially in the areas closer to the bearing lips. Glancing angle

implantation not only gives rise to a smaller projected range, but also results in more severe sputtering as well. It should be mentioned that the effects are less serious in the center of the grooves, but nonetheless, both our experimental and simulation results suggest the use of a shorter pulse duration as well as higher plasma density for more uniform and efficient implantation.

V. Conclusion

Our experimental results reveal retained dose and projected range variations along the two races of a ball bearing assembly. For the outward-facing race of the inner piece, a higher retained dose is observed near the groove center, but the exact location depends on the implantation conditions. The groove edges receive a lower dose, and the implantation depth is shallower. Because of the horizontal placement of the bearing on the sample plate, the upper side of the groove receives a smaller ion dose compared with the lower side. For the inward-facing race of the outer ring, the maximum retained dose is also observed in the middle of the groove. A high plasma density, small pulse duration condition yields better implant uniformity. Our simulation results based on a fluid model point to the advantage of the better conformality of a thinner plasma sheath. The nonuniformity is improved to 35% and generally acceptable to the aerospace industry.

References

[1] J. R. Conrad, J. L. Radtke, R. A. Dodd, F. J. Worzala, and N. C. Tran, "Plasma source ion implantation technique for surface modification of materials," *J. Appl. Phys.*, vol. 62, no. 11, pp. 4591–4596, 1987.

[2] G. A. Collins, R. Hutchings, J. Tendys, and M. Samandi, "Advanced surface treatments by plasma ion implantation," *Surf. Coat. Technol.*, vol. 68/69, pp. 285–293, 1994.

[3] J. R. Conrad, R. A. Dodd, S. Han, M. Madapura, J. Scheuer, K. Sridharan, and F. J. Worzala, "Ion beam assisted coating and surface modification with plasma source ion implantation," *J. Vac. Sci. Technol. A*, vol. 8, no. 4, pp. 3146–3151, 1990.

[4] S. Y. Wang, P. K. Chu, B. Y. Tang, X. C. Zeng, and X. F. Wang, "Improvement of the corrosion property of Cr4Mo4V bearing steel using plasma immersion ion implantation," *Nucl. Instrum. Methods B*, vol. 127/128, pp. 1000–1003, 1997.

[5] P. A. Watterson, "Child–Langmuir sheath structure around wedge-shaped cathods," *J. Phys. D: Appl. Phys.*, vol. 22, pp. 1300–1307, 1989.

[6] J. T. Sheuer, M. Shamin, and J. R. Conrad, "Model of plasma source ion implantation in planar, cylindrical and spherical geometries," *J. Appl. Phys.*, vol. 67, no. 3, pp. 1241–1245, 1990.

[7] T. E. Sheridan, "Sheath expansion at a corner," *J. Phys. D: Appl. Phys.*, vol. 29, pp. 2725–2728, 1996.

[8] M. Hong and G. A. Emmert, "Two-dimensional fluid simulation of expanding plasma sheaths," *J. Appl. Phys.*, vol. 78, no. 12, pp. 6967–6973, 1995.

[9] S. M. Malik, D. E. Muller, K. Sridharan, R. P. Fetherston, and N. Tran, "Distribution of incident ions and retained dose analysis for a wedge-shaped target in plasma source ion implantation," *J. Appl. Phys.*, vol. 77, no. 3, pp. 1015–1019, 1995.

[10] J. Hartmann, W. Ensinger, R. W. Thomae, H. Bender, A. Koniger, B. Stritzker, and B. Rauschenbach, "Lateral implantation dose measurements of plasma immersion ion implanted nonplanar samples," *Nucl. Instrum. Methods B*, vol. 112, pp. 255–258, 1996.

[11] T. Hochbauer, W. Ensinger, G. Schrag, J. Hartmann, B. Stritzker, and B. Rauschenbach, "Homogeneity measurements of plasma immersion ion-implanted complex-shaped samples," *Nucl. Instrum. Methods B*, vol. 127/128, pp. 869–872, 1997.

[12] S. Mandl, H. Reuther, J. Brutscher, R. Gunzel, and W. Moller, "Measured and calculated dose distribution for 2-D plasma immersion ion implantation," *Surf. Coat. Technol.*, vol. 93, pp. 229–233, 1997.

[13] P. K. Chu, B. Y. Tang, Y. C. Cheng, and P. K. Ko, "Principles and characteristics of a new generation plasma immersion ion implanter," *Rev. Sci. Instrum.*, vol. 68, no. 4, pp. 1866–1874, 1997.

[14] Z. M. Zeng, X. B. Tian, D. T. K. Kwok, B. Y. Tang, and P. K. Chu, "Influence of sample placement on the dose uniformity in plasma immersion ion implantation of industrial ball bearings," *IEEE Trans. Plasma Sci.*, vol. 27, pp. 1203–1209, Aug. 1999.

[15] M. Widner, I. Alexeff, and W. D. Jones, "Ion acoustic wave excitation and ion sheath evolution," *Phys. Fluids*, vol. 13, no. 10, pp. 2532–2537, 1970.

[16] T. E. Sheridan and M. J. Alport, "Ion-matrix sheath around a square bar," *J. Vac. Sci. Technol. B*, vol. 12, no. 2, pp. 897–900, 1994.

[17] ——, "Two-dimensional model of ion dynamics during plasma source ion implantation," *Appl. Phys. Lett.*, vol. 64, no. 14, pp. 1783–1785, 1994.

[18] T. E. Sheridan, "Sheath expansion into a large bore," *J. Appl. Phys.*, vol. 80, no. 1, pp. 66–69, 1993.

[19] M. Hong and G. A. Emmert, "Two-dimensional fluid modeling of time-dependent plasma sheaths," *J. Vac. Sci. Technol. B*, vol. 12, no. 2, pp. 889–896, 1994.

[20] P. L. Devries, *A First Course in Computational Physics*. New York: Wiley Press, 1994, p. 368.

[21] Z. M. Zeng, T. K. Kwok, X. B. Tian, B. Y. Tang, and P. K. Chu, "Investigation of dose uniformity on the inner races of bearings treated by plasma immersion ion implantation," *J. Appl. Phys.*, vol. 86, no. 1, pp. 120–123, 1999.

Zhaoming Zeng received the B.S. and M.S. degrees in materials science from the Harbin Institute of Technology (HIT), China, in 1990 and 1993, respectively. He received the Ph.D. degree at HIT.

From 1993 to 1996, he worked for Attech Electronics Ltd., Hong Kong, and was in charge of production development and management. In July 1998, he joined the Plasma Laboratory of the City University of Hong Kong as a Research Assistant. His research interests include surface modification of materials, numerical simulation of plasma immersion ion implantation, and plasma-processing equipment technology.

Paul K. Chu (SM'97) received the B.S. degree in mathematics from Ohio State University, Columbus, in 1977 and the M.S. and Ph.D. degrees in chemistry from Cornell University, Ithaca, NY, in 1979 and 1982, respectively.

He joined Charles Evans & Associates, CA, in 1982 and assumed various technical and managerial positions. He founded Evans Asia in early 1990 and later joined the City University of Hong Kong as a Visiting Faculty Member. He is currently Professor in the Department of Physics and Materials Science, City University of Hong Kong. He also holds concurrent professorships at Fudan University, Peking University, Southwest Jiaotong University, and Southwestern Institute of Physics in China. His research activities include plasma-processing technology and materials characterization.

Dr. Chu is a member of the American Chemical Society and the Materials Research Society. He is a Fellow of the Hong Kong Institution of Engineers and an Elected Member of the Böhmische Physical Society.

Xiubo Tain was born in 1969. He received the B.S. and M.S. degrees in materials science and technology from the Harbin Institute of Technology (HIT), China, in 1990 and 1993, respectively. He is currently pursuing the Ph.D. degree at the City University of Hong Kong.

He joined the Plasma Laboratory of the City University of Hong Kong in July 1998 as a Research Assistant. His research interests include low-energy, high-frequency plasma immersion ion implantation, plasma and nitriding equipment and applications, and *in situ* monitoring in plasma immersion ion implantation.

Baoyin Tang received a degree from the Department of Engineering Physics, Harbin Institute of Technology (HIT), China, in 1960.

He is a Professor and the Director of the Surface Modification of Materials Group in the Advanced Welding & Production Technology National Key Laboratory, HIT. He was engaged in teaching on electrical physics and research on accelerators, ion sources, and ion implantation before 1990. He worked with Prof. J. R. Conrad in the Plasma Source Ion Implantation Group, University of Wisconsin-Madison, to study plasma-based ion implantation and surface modification of advanced materials from April 1990 to December 1992. He has been working with Prof. P. K. Chu in the Department of Physics and Materials Science, City University of Hong Kong, since 1995. His research interests include development of multipurpose PIII equipment, improvement of PIII techniques, and industrial applications. In recent years, he has published more than 40 scientific and technical papers in international academic conferences and journals.

Dixon Tat-Kun Kwok (M'97) received the B.Sc. degree in physics in 1988 and the Ph.D. degree in solid state physics in 1993 from King's College London, University of London.

He served as a Postdoctoral Fellow (April 1994–March 1995) at the Surface Physics Laboratory of Fudan University, Shanghai. In April 1995, he became a Research Associate (April 1995–June 1996) of the Physics Department of the Hong Kong University of Science and Technology in Hong Kong. Recently, he has become a Research Fellow (July 1996–present) in the Department of Physics and Material Science, City University of Hong Kong. He has published papers on topics related to photoluminescence and photoabsorption of point defects in silicon, reflectance difference spectroscopy, and numerical simulation of plasma immersion ion implantation.